

Analysis of electro-osmotic flow in a microchannel with undulated surfaces

Hiroaki Yoshida^{a,b,*}, Tomoyuki Kinjo^{a,b}, Hitoshi Washizu^{a,b}

^aToyota Central R&D Labs., Inc., Nagakute, Aichi 480-1192, Japan

^bElements Strategy Initiative for Catalysts and Batteries (ESICB), Kyoto University, Kyoto 615-8245, Japan

Abstract

The electro-osmotic flow through a channel between two undulated surfaces induced by an external electric field is investigated. The gap of the channel is very small and comparable to the thickness of the electrical double layers. A lattice Boltzmann simulation is carried out on the model consisting of the Poisson equation for electrical potential, the Nernst–Planck equation for ion concentration, and the Navier–Stokes equations for flows of the electrolyte solution. An analytical model that predicts the flow rate is also derived under the assumption that the channel width is very small compared with the characteristic length of the variation along the channel. The analytical results are compared with the numerical results obtained by using the lattice Boltzmann method. In the case of a constant surface charge density along the channel, the variation of the channel width reduces the electro-osmotic flow, and the flow rate is smaller than that of a straight channel. In the case of a surface charge density distributed inhomogeneously, one-way flow occurs even under the restriction of a zero net surface charge along the channel.

Keywords: Electro-osmotic flow, Electrical double layer, Lattice Boltzmann method, Lubrication approximation theory

1. Introduction

Adjacent to the interface between an electrolyte solution and a charged solid surface, an electrical double layer is formed. The thickness of the double layer ranges from a few nanometers to hundreds of nanometers, depending on the salt concentration. Since the ion concentration in the electrical double layer is highly inhomogeneous and the local charge neutrality is broken, interaction with an externally applied electric field can cause a driving force acting on the electrolyte solution. The driving force is the main factor for electrokinetic effects, such as the electro-migration of colloid particles and the electro-osmotic flow inside microchannels [1, 2], which are especially conspicuous in small-scale systems.

Micro- and nano-fabrication techniques have developed greatly in recent years, and so researchers have been able to control and use electrokinetic phenomena in engineering applications. For example, an electro-osmotic pump without moving parts [3, 4] and an energy-harvesting device using the driving force induced by the salt-concentration gradient [5] have been proposed very recently. Along with the expectations for engineering applications, fundamental research relevant to electrokinetic phenomena in small-scale systems, ranging from nano- to micrometers, has also attracted attention [6–15]. Particularly, the advances in observing and processing techniques have prompted research focusing on surface properties such as roughness and structure [16–23].

In the present study, to clarify the effects of surface properties on electrokinetic phenomena, we investigate electro-osmotic

flows between two surfaces, which have a periodic structure and a non-uniform charge distribution, by means of both numerical and analytical approaches. The numerical analysis is based on the coupled lattice Boltzmann method for solving the Navier–Stokes equations, the Nernst–Planck equation, and the Poisson equation [24]. The numerical solutions to these equations, i.e., the electrolyte flow, the ion concentrations, and the electrical field, are directly obtained. In the analytical approach, the lubrication approximation theory [25–27] is applied to the system with electrical double layers of finite thickness, to derive a model equation that predicts the flow rate under the assumption of moderate variation of the surface structure along the channel. With these approaches, we investigate the electro-osmotic flow in microchannels formed by the surfaces that are undulated and (a) charged negatively at a constant surface charge density or (b) charged non-uniformly along the channel such that the net surface charge vanishes. For both cases, the electro-osmotic flow rate is evaluated and the dependency on geometrical parameters, such as the amplitude of the surface shape, is discussed.

2. Problem and basic equations

2.1. Channel with undulated surfaces

Let us consider a channel between two walls, each of which has a periodic structure of period L in the x direction. The positions of the interfaces are expressed as $y = \pm h(x)$ (Fig. 1). The surface charge density on the channel walls is assumed to be a given function $\sigma(x)$. The two-dimensional domain between the surfaces ($-h(x) < y < h(x)$) is filled with a 1 : 1 electrolyte solution, and the electrical double layer is formed near the interfaces. We investigate the electro-osmotic flow caused

*Corresponding author.

Email address: h-yoshida@mosk.tytlabs.co.jp (Hiroaki Yoshida)

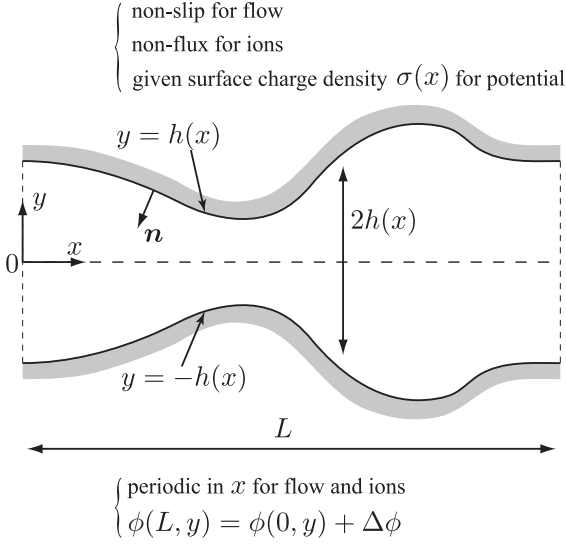


Figure 1: Geometry of the problem.

by an electrical field applied in the x direction by applying the governing equations described in the next subsection.

2.2. Governing equations

We assume a Newtonian fluid for the electrolyte solution, and then the flow is described by the Navier–Stokes equations:

$$\frac{\partial u_j}{\partial x_j} = 0, \quad (1)$$

$$\frac{\partial u_i}{\partial t} + u_j \frac{\partial u_i}{\partial x_j} = -\frac{1}{\rho_0} \frac{\partial p}{\partial x_i} + \nu \frac{\partial^2 u_i}{\partial x_j^2} + \frac{F_i}{\rho_0}, \quad (2)$$

where t is the time and \mathbf{x} is the spatial coordinate. In the present paper, we use either boldface letters or assign indexes i and j to designate vector elements. The summation convention is assumed for repeated indexes. The functions $\mathbf{u}(t, \mathbf{x})$ and $p(t, \mathbf{x})$ are the flow velocity and the pressure of the electrolyte solution, respectively, and $\mathbf{F}(t, \mathbf{x})$ is the body force per unit volume. The density ρ_0 and the kinematic viscosity ν of the electrolyte solution are assumed to be constant.

The mass conservation equation for the ion species is written as

$$\frac{\partial C_m}{\partial t} + \frac{\partial J_{mj}}{\partial x_j} = 0, \quad (3)$$

$$J_{mi} = -\frac{e z_m D_m}{k_B T} C_m \frac{\partial \phi}{\partial x_i} - D_m \frac{\partial C_m}{\partial x_i} + C_m u_i, \quad (4)$$

where C_m and \mathbf{J}_m denote the concentration and the flux of an ion, respectively, with $m = a$ for the anion and $m = c$ for the cation. Here, e is the unit charge, k_B is Boltzmann's constant, and T is the temperature. The constants z_m and D_m are the valence and the diffusion coefficient of species m , respectively. Equation (4) is referred to as the Nernst–Planck model [28], where the first, second, and third terms on the right-hand side

of the flux equation are the contributions of electrochemical migration, diffusion, and convection of the electrolyte solution, respectively.

Finally, the electrical potential ϕ is governed by the following Poisson equation:

$$\varepsilon \frac{\partial^2 \phi}{\partial x_j^2} = -\rho_e, \quad (5)$$

where ε is the dielectric constant of the electrolyte solution. The local charge density ρ_e is defined in terms of the ion concentration as

$$\rho_e = \sum_m F z_m C_m, \quad (6)$$

where F is Faraday's constant. With this local charge density, the body force \mathbf{F} in Eq. (2) is defined as the interaction with the electric field:

$$F_i = -\rho_e \frac{\partial \phi}{\partial x_i}. \quad (7)$$

If the convection term in Eq. (4) is negligible compared with the other two terms and a unique value of potential is defined at $C_m = C_0$, integration of Eq. (4) yields the Boltzmann distribution $C_m = C_0 \exp(-e z_m \phi / k_B T)$. With this formula, Eq. (5) reduces to the Poisson–Boltzmann equation. In the electrokinetic flows considered in the present paper, however, although the convection term is sufficiently small, specifying a unique potential value at $C_m = C_0$ is difficult because of the external potential gradient. We therefore apply the original set of equations described here in the numerical simulations in Section 5. Then the ion distribution affected by the external potential is obtained as shown in Section 5.2, which the Poisson–Boltzmann equation decoupled from the external potential field fails to capture.

2.3. Boundary conditions on solid-liquid interface

For the flow velocity, the ordinary non-slip condition is assumed at the solid-liquid interface:

$$u_i = 0, \quad \text{at } y = \pm h(x). \quad (8)$$

Note that in nano-scale flows, the simple non-slip condition is not sufficient and so a model describing the slip taking place at the interface is necessary. However, since the scale of the problems considered in the present paper is relatively large (at a scale of micrometers), we assume the non-slip condition to be valid. For the ion concentration, no flux goes across the boundary, which is formulated simply as

$$n_j J_j = 0, \quad \text{at } y = \pm h(x), \quad (9)$$

where \mathbf{n} is the unit normal vector pointing inward to the fluid region. If we substitute Eq. (4) into Eq. (9), then we have

$$-\frac{e z_m D_m}{k_B T} C_m n_j \frac{\partial \phi}{\partial x_j} - D_m n_j \frac{\partial C_m}{\partial x_j} + C_m n_j u_j = 0. \quad (10)$$

This form of the Neumann-type boundary condition seems rather complex to implement in the lattice Boltzmann method. However, with the scheme for the Nernst–Planck model described in

the next section we can impose this condition in a simple manner. Finally, the boundary conditions for the electrical potential are given as the following Neumann-type condition:

$$-\varepsilon n_j \frac{\partial \phi}{\partial x_j} = \sigma, \quad \text{at } y = \pm h(x). \quad (11)$$

3. Lattice Boltzmann method

3.1. Lattice Boltzmann equation

In this subsection, we outline the numerical method based on the lattice Boltzmann method (LBM) [29–33] for solving the following set of model equations for electrokinetic flows: (I) the Poisson equation (5) with Eq. (6), (II) the Nernst–Planck equation (3) with Eq. (4), and (III) the Navier–Stokes equations (2) with Eqs. (1) and (7).

The four lattice Boltzmann equations are assigned to the unknown variables ϕ , C_a , C_c , and \mathbf{u} . First, the lattice Boltzmann algorithm generally used for (I) through (III) is outlined, and then we comment on the scheme for the Nernst–Planck equation. The complete description of the framework including the rules for the boundary conditions is found in Ref. [24].

The LBM tracks the behavior of the distribution function $f_\alpha(t, \mathbf{x})$, where $\alpha = 0, 1, 2, \dots, N$, rather than that of the unknown variable for the target partial differential equations. Here and in what follows, the subscript α is used to indicate the quantities corresponding to the directions of the discrete velocities, such as f_α above. The values of the distribution function travel over a regular spatial lattice with the assigned discrete velocities, of which the direction is defined in terms of the vector \mathbf{e}_α . The explicit expression of the vector \mathbf{e}_α depends on the type of partial differential equation to be solved.

Since we have four unknown variables, namely the electrical potential, the concentration of cation and anion, and the flow velocity, we use four distribution functions, denoted by f_α^s with $s = p, c, a, \text{ and } u$. The unknown variables are calculated as moments of the distribution function:

$$\phi = \sum_\alpha f_\alpha^p, \quad (12)$$

$$C_c = \sum_\alpha f_\alpha^c, \quad C_a = \sum_\alpha f_\alpha^a, \quad (13)$$

$$u_i = \frac{\Delta x}{\rho \Delta t} \sum_\alpha e_{\alpha i} f_\alpha^u, \quad \text{with } \rho = \sum_\alpha f_\alpha^u, \quad (14)$$

where Δt and Δx are the time step and the grid interval, respectively.

The lattice Boltzmann equation used in the present study is written as

$$f_\alpha^s(t + \Delta t, \mathbf{x} + \mathbf{e}_\alpha \Delta x) - f_\alpha^s(t, \mathbf{x}) = \frac{1}{\tau^s} (f_\alpha^{s(\text{eq})} - f_\alpha^s(t, \mathbf{x})) + \frac{\Delta t}{2} (g_\alpha^s(t, \mathbf{x}) + g_\alpha^s(t, \mathbf{x} + \mathbf{e}_\alpha \Delta x)), \quad (15)$$

where the function g_α^u corresponds to the forcing term for solving the Navier–Stokes equations, and g_α^p corresponds to the source term for solving the Poisson equation, while $g_\alpha^c = g_\alpha^a =$

0. Note that, in our formulation, \mathbf{e}_α is defined as a dimensionless vector designating the directions of the discrete velocities [24]. The first term on the right-hand side is the collision term, which defines the relaxation process during a time step. The coefficient τ^s defines the relaxation time and is related to the dielectric constant, the diffusion coefficients, and the viscosity [24]:

$$\tau^p = \frac{1}{2} + \frac{\Delta t}{\Delta x^2 \Lambda^p} \varepsilon, \quad \tau^{c,a} = \frac{1}{2} + \frac{\Delta t}{\Delta x^2 \Lambda^{c,a}} D_{c,a}, \quad \tau^u = \frac{1}{2} + \frac{\Delta t}{\Delta x^2 \Lambda^u} \nu, \quad (16)$$

where the value of constant Λ^s depends on the discrete velocity set \mathbf{e}_α [24]. The equilibrium distribution function $f_\alpha^{s(\text{eq})}$ is expressed in terms of the local value of the physical quantities, such as the electrical potential, the ion concentration, and the flow velocity. The collision term used herein is the single-relaxation-time (SRT) method, in which a common value of the relaxation-time coefficient τ^s is assigned to all directions of α . Although various types of collision operator have been presented to increase stability and/or accuracy [33–37], we prefer the simplicity of the SRT for the present study, because the geometrical setup and the parameters used in Section 5 are not very severe. The extension of the present numerical framework to the one using the multiple-relaxation-time collision operator, which exhibits robustness for severe parameter set, is straightforward, if the techniques described in Refs. [33, 34, 38, 39] are applied. The complete definitions of \mathbf{e}_α , $f_\alpha^{s(\text{eq})}$ and g_α^s are found in Ref. [24].

To implement the LBM, Eq. (15) is split into the collision process and the streaming process, and the distribution function is updated in an explicit manner:

Collision:

$$\hat{f}_\alpha^s(t, \mathbf{x}) = f_\alpha^s(t, \mathbf{x}) + \frac{1}{\tau^s} (f_\alpha^{s(\text{eq})} - f_\alpha^s(t, \mathbf{x})) + \frac{\Delta t}{2} g_\alpha^s(t, \mathbf{x}), \quad (17)$$

Streaming:

$$f_\alpha^s(t + \Delta t, \mathbf{x} + \mathbf{e}_\alpha \Delta x) = \hat{f}_\alpha^s(t, \mathbf{x}) + \frac{\Delta t}{2} g_\alpha^s(t, \mathbf{x} + \mathbf{e}_\alpha \Delta x). \quad (18)$$

In solving the Navier–Stokes equations, the simple halfway bounce-back rule for the non-slip boundary condition is applied regarding the lattice points outside the channel as the solid phase. Similarly, the halfway bounce-back rule for the non-flux boundary condition is utilized in solving the Nernst–Planck equation. On the other hand, a modified boundary rule for the curved Neumann boundary condition is applied for solving the Poisson equation. This is because the simple bounce-back rule causes serious errors when implementing the curved Neumann boundary condition with inhomogeneous term (Eq. (11)), and special treatment is necessary, as demonstrated in Refs. [39–41]. In the present study, the scheme utilizing the level set method described in detail in Ref. [39] is employed, because the implementation is rather simple once the level set function describing the surface shape is constructed.

Strictly speaking, the numerical solution \mathbf{u} obtained with the LBM includes an artificial compressibility, and different formulations have been proposed to deal with this matter (e.g.,

Ref. [42]). We employ, however, the most widely used formulation for the equilibrium distribution function (e.g., Refs. [24, 31]) suffering from the artificial compressibility. Since the variation of ρ (or p) is controlled to remain small (by setting small Mach number $|\mathbf{u}|\Delta t/\Delta x$) so that the incompressible Navier–Stokes equations are well approximated [43], we safely apply this method to obtain the flow field in the present analysis.

We further comment on the scheme used for solving the Nernst–Planck equation: The electrochemical migration term (the first term on the right-hand side of Eq. (4)) is often regarded as the source term [44], i.e., the function g_α^s is defined to include the migration effect. Although this is a straightforward strategy of dealing with this term in the LBM, it causes difficulty in implementing the Neumann-type boundary condition given in Eq. (10) directly. To circumvent this difficulty, we use the equilibrium distribution function $f_\alpha^{s(\text{eq})}$ rather than the source term to incorporate the electrical migration. In the description of \mathbf{J}_m in Eq. (4), we are able to regard the coefficient of C_m in the migration term as a part of the convection velocity of the general convection-diffusion equation. Accordingly, the equilibrium distribution function of the LBM for the general convection-diffusion equation described in Ref. [39] is defined as

$$f_\alpha^{s(\text{eq})} = \left[\omega_\alpha^s + \frac{\Delta t}{\Delta x \Lambda^s} \left(u_j - \frac{e z_m D_m}{k_B T} \frac{\partial \phi}{\partial x_j} \right) e_{\alpha j} \omega_\alpha^s \right] C_m, \quad (19)$$

where $s = m (= c \text{ and } a)$ and ω_α^s is the weight coefficient and Λ^s is defined as $\sum_\alpha \omega_\alpha^s e_{i\alpha} e_{j\alpha} = \Lambda^s \delta_{ij}$ with δ_{ij} being Kronecker’s delta. The actual values for ω_α^s are given in Ref. [24]. Since the value of $\partial\phi/\partial x$ is evaluated locally [24, 39], the communication with the surrounding grid points is achieved only through the streaming process (Eq. (18)). This locality enables us to implement the original boundary condition for the ion flux given in Eq. (10) in a natural form by using the standard bounce-back rules. The artificial flux in time-dependent problems observed in using the source-term scheme is also properly eliminated. (See Ref. [24] for a comparison with a previous source-term scheme.) Among the LBMs developed for similar systems [11, 17, 44–50], we prefer to use the present algorithm because of this simple treatment of the Nernst–Planck equation.

3.2. Coupling procedure

The set of model equations includes the Poisson equation independent of time, in which the numerical solution ϕ is obtained as the long-time limit of the time-dependent solution of the diffusion equation. We thus introduce an artificial time axis \tilde{t} for the iteration process for solving the Poisson equation. On the other hand, the ion concentrations (C_a and C_c) and the flow velocity \mathbf{u} of the electrolyte solution are obtained by using the common time axis t .

As demonstrated in Ref. [51], in solving the Poisson equation, the long-time limit of the diffusion equation can lead to an undesired solution if the initial condition is inappropriate. In the present work, a linear profile in the x -direction corresponding to the potential bias is used as an initial condition for the \tilde{t} -loop at the very first step in physical time $t = 0$. Then such

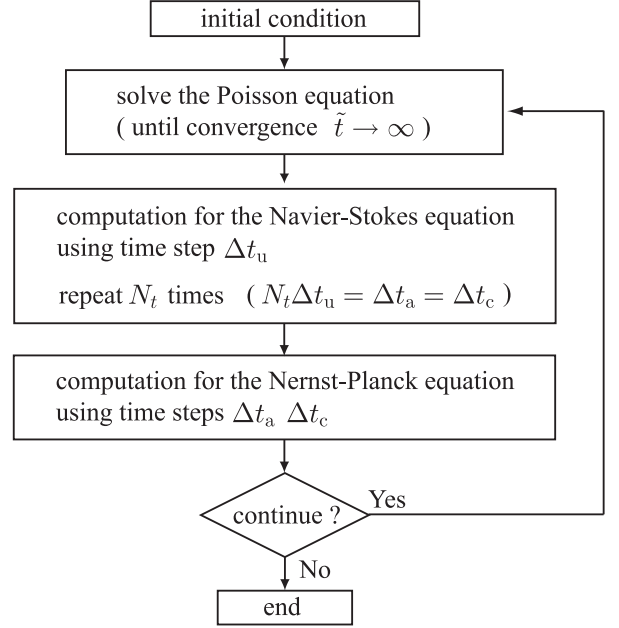


Figure 2: Computational procedure for the coupled LBM.

undesired solution is not encountered in the numerical simulations presented in Section 5. We must note here that, as is well known, the convergence in reaching the steady state in \tilde{t} is very slow. For $t > 0$ the potential field at the previous time step is used as an initial guess for the loop in \tilde{t} , and then the number of time steps required to obtain the potential field at each time step in t is greatly reduced. The very slow convergence in \tilde{t} -loop at the initial stage in t would be efficiently accelerated if one uses a promising method employing the multigrid technique as proposed in Ref. [52].

Since the timescales of each transport phenomenon are different, we need to assign different values to the time step Δt . Here, we denote the time steps for the anion, cation, and flow velocity by Δt_a , Δt_c , and Δt_u , respectively. The kinematic viscosity is normally much larger than the diffusion coefficients of the ion species, i.e., the Schmidt number defined as $Sc = \nu/D_m$ is large. Therefore the timescale of the flow is shorter than that of the diffusion process, i.e., $\Delta t_u \ll \Delta t_a, \Delta t_c$. We show in Fig. 2 the iterative procedure for the case of $N_t \Delta t_u = \Delta t_a = \Delta t_c$, which is the case discussed in Section 5 where $Sc \sim 90$ and thus $N_t = 100$ is chosen. At each instance in t , the electrical potential ϕ is obtained as the limit at which $\tilde{t} \rightarrow \infty$. Practically, however, the iteration with respect to \tilde{t} is terminated when the difference between two successive values of ϕ reaches a certain tolerance, typically 10^{-7} V, at all of the lattice points.

4. Analytical model based on the lubrication approximation theory

In this section, we outline the procedure to obtain an analytical model for the electro-osmotic flow rate. The method of analysis is based on the lubrication approximation theory, which was first applied to the electro-osmotic flow in Ref. [25]

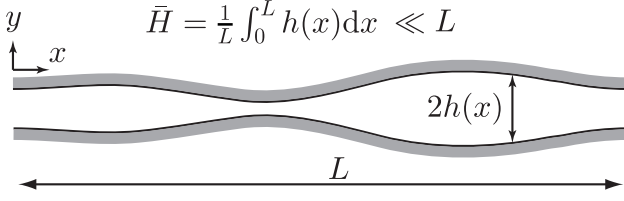


Figure 3: Lubrication approximation.

for the case of a very thin electrical double layer, where the Helmholtz–Smoluchowski approximation was assumed. To simplify the set of model equations described in Section 2 such that the analytical method is applicable, we assume the following: (i) steady flow, (ii) small convection effect in Eq. (4) (the third term on the right-hand side) compared with the other two terms, (iii) small zeta potential (the electrical potential at the interface) so that the Debye–Hückel approximation is valid, and (iv) larger length scale for the variation of the surface structure and of the surface charge density along the channel than the channel width, as depicted in Fig. 3 ($\bar{H} \ll L$; $\bar{H} = (1/L) \int_0^L h(x) dx$). Assumption (iv) results in $\delta = \bar{H}/L \ll 1$ and this parameter δ is used as a small parameter in the expansion analysis of the lubrication approximation theory.

Before discussing the expansion analysis, we introduce the following dimensionless variables:

$$x = \tilde{x}L, \quad y = \tilde{y}\bar{H}, \quad \mathbf{u} = \tilde{\mathbf{u}}u_0, \quad (20)$$

$$p = \tilde{p} \left(\frac{\mu u_0 L}{\bar{H}^2} \right), \quad \phi_e = \tilde{\phi}_e \left(\frac{\bar{H} \sigma_0}{\varepsilon} \right), \quad \phi_* = \tilde{\phi}_* \Delta \phi, \quad (21)$$

$$h(x) = \tilde{h}(\tilde{x})\bar{H}, \quad \sigma(x) = \tilde{\sigma}(\tilde{x})\sigma_0, \quad (22)$$

where the reference flow velocity u_0 and the inverse Debye length κ are defined as

$$u_0 = \left(\frac{\kappa^2 \bar{H}^3 \sigma_0 \Delta \phi}{\mu L} \right), \quad \kappa = \left(\frac{2C_0 F e}{\varepsilon k_B T} \right)^{1/2}, \quad (23)$$

and $\mu = \nu \rho_0$ is the viscosity of the electrolyte solution, C_0 is the reference value of the ion concentration, σ_0 is the reference value of the surface charge density, and $\Delta \phi$ is the potential difference between $x = 0$ and $x = L$ (Fig. 1). Because the Debye–Hückel approximation is assumed and the Poisson equation is hence linearized, the electrical potential is split into the equilibrium potential ϕ_e and the potential describing the external electric field ϕ_* .

Using the variables defined in Eqs. (20) through (22), we transform the governing equations into a dimensionless form. Here and in the following, the tilde attached to the dimensionless variables is dropped for simplicity, unless otherwise stated.

The set of equations then reads

$$\delta^2 \frac{\partial^2 \phi_*}{\partial x^2} + \frac{\partial^2 \phi_*}{\partial y^2} = 0, \quad (24)$$

$$\delta^2 \frac{\partial^2 \phi_e}{\partial x^2} + \frac{\partial^2 \phi_e}{\partial y^2} = (\bar{H}\kappa)^2 \phi_e, \quad (25)$$

$$0 = -\frac{\partial p}{\partial x} + \delta^2 \frac{\partial^2 u_x}{\partial x^2} + \frac{\partial^2 u_x}{\partial y^2} + \phi_e \frac{\partial \phi_*}{\partial x} + \gamma \delta \phi_e \frac{\partial \phi_e}{\partial x}, \quad (26)$$

$$0 = -\frac{1}{\delta} \frac{\partial p}{\partial y} + \delta^2 \frac{\partial^2 u_y}{\partial x^2} + \frac{\partial^2 u_y}{\partial y^2} + \frac{1}{\delta} \phi_e \frac{\partial \phi_*}{\partial y} + \gamma \phi_e \frac{\partial \phi_e}{\partial y}, \quad (27)$$

where $\gamma = \sigma_0 L / \varepsilon \Delta \phi$. The boundary conditions at $y = \pm h(x)$ are

$$n_x \delta \frac{\partial \phi_*}{\partial x} + n_y \frac{\partial \phi_*}{\partial y} = 0, \quad (28)$$

$$n_x \delta \frac{\partial \phi_e}{\partial x} + n_y \frac{\partial \phi_e}{\partial y} = -\sigma, \quad (29)$$

$$u_x = u_y = 0, \quad (30)$$

where the components of the normal vector at the surfaces are expressed as $n_x = \pm \delta h' / (1 + \delta^2 h'^2)^{1/2}$ and $n_y = \mp 1 / (1 + \delta^2 h'^2)^{1/2}$, with h' being the derivative of $h(x)$. Here, the Nernst–Planck equation has been integrated under assumptions (i) and (ii) described above to have the Boltzmann distribution for the ion concentration, and has been further simplified under assumption (iii) to be incorporated as in Eqs. (25) through (27).

To analyze the boundary-value problem described above, we expand the variables with respect to the small parameter δ :

$$\phi_* = \phi_*^{(0)} + \delta \phi_*^{(1)} + \delta^2 \phi_*^{(2)} + \dots, \quad (31)$$

$$\phi_e = \phi_e^{(0)} + \delta \phi_e^{(1)} + \delta^2 \phi_e^{(2)} + \dots, \quad (32)$$

$$\mathbf{u} = \mathbf{u}^{(0)} + \delta \mathbf{u}^{(1)} + \delta^2 \mathbf{u}^{(2)} + \dots, \quad (33)$$

$$p = p^{(0)} + \delta p^{(1)} + \delta^2 p^{(2)} + \dots. \quad (34)$$

The goal of this analysis is to obtain the solution describing the electro-osmotic flow for the limit of $\delta \rightarrow 0$, i.e., the solution $u_x^{(0)}$. After substituting the expansions into Eqs. (24) through (27), we equate the terms of the same power of δ to obtain the series of equations and boundary conditions for the coefficients in the expansion, such as $\phi_*^{(n)}$ and $\mathbf{u}^{(n)}$. The series of boundary-value problems are solved from the lowest order.

We first analyze the boundary-value problems for $\phi_*^{(n)}$ resulting from Eqs. (24) and (28). The analysis up to the order of δ^2 yields the following expression for $\phi_*^{(0)}$:

$$\frac{\partial \phi_*^{(0)}}{\partial x} = \frac{1}{w_1 h}, \quad \frac{\partial \phi_*^{(0)}}{\partial y} = 0, \quad (35)$$

where w_1 is a quantity defined via

$$w_k = \int_0^1 \tilde{h}(\tilde{x})^{-k} d\tilde{x}. \quad (36)$$

In Eq. (36), the tilde explicitly shows that \tilde{h} and \tilde{x} are dimensionless. Turning to the analysis of the boundary-value problems derived from Eqs. (25) and (29), the solution $\phi_e^{(0)}$ is readily obtained from the leading-order analysis as

$$\phi_e^{(0)} = \frac{\sigma \cosh(\kappa \bar{H} y)}{\kappa \bar{H} \sinh(\kappa \bar{H} h)}. \quad (37)$$

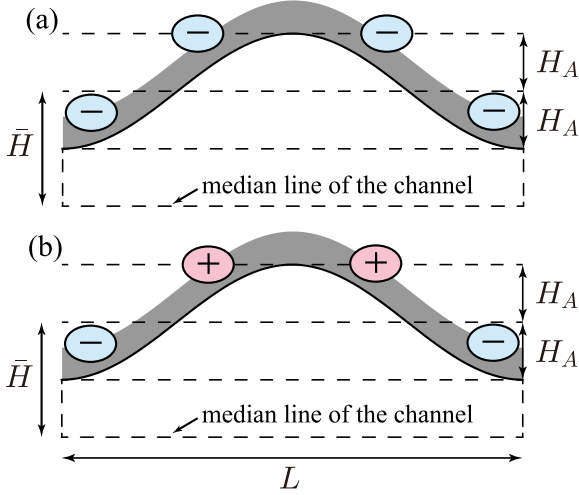


Figure 4: Schematic diagram of the surface shape and the charge distribution.

We next analyze the leading-order problem derived from Eq. (27). From the result shown in Eq. (35), we find that $p^{(0)}$ only depends on x :

$$\frac{\partial p^{(0)}}{\partial y} = 0. \quad (38)$$

The leading-order problem that results from Eqs. (26) and (30) is then considered. Using all the results in Eqs. (35) through (38), we arrive at the following expression for $u_x^{(0)}$:

$$u_x^{(0)} = \frac{1}{2} \frac{\partial p^{(0)}}{\partial x} (y^2 - h^2) + \frac{\sigma}{w_1 h (\kappa \bar{H})^3} (\cosh(\kappa \bar{H} h) - \cosh(\kappa \bar{H} y)). \quad (39)$$

The electro-osmotic flow rate is obtained by integrating this expression over the channel width, i.e., $Q = 2 \int_0^h u_x dy$. However, the unknown variable $\partial p^{(0)}/\partial x$ is still included in this expression. The unknown variable is eliminated by using the constraint of the periodic boundary condition for the pressure field, i.e., $\int_0^L (\partial p^{(0)}/\partial x) dx = 0$. Then, we obtain the explicit formula for the electro-osmotic flow rate in the limit of $\delta \rightarrow 0$ as follows:

$$Q = \frac{2\sigma_0 \Delta\phi}{\mu \kappa^2 L w_1 w_3} \int_0^1 \frac{\tilde{\sigma}(\tilde{x})}{\tilde{h}(\tilde{x})^3} \left(\frac{\kappa \bar{H}}{\tanh(\kappa \bar{H} \tilde{h})} - \frac{1}{\tilde{h}} \right) d\tilde{x}, \quad (40)$$

where w_1 and w_3 are dimensionless quantities defined in Eq. (36). Here, the tilde is explicitly shown on the dimensionless variables \tilde{x} , \tilde{h} , and $\tilde{\sigma}$ defined in Eqs. (20) and (22), whereas Q denotes the dimensional volumetric flow rate per unit length in the z direction.

5. Results and discussion

5.1. Constant surface charge density

The electro-osmotic flow through channels with the sinusoidal surfaces, as depicted in Fig. 4, is considered in the present

study. More precisely, the shape of the surfaces is defined as

$$h(x) = \bar{H} - H_A \cos\left(\frac{2\pi x}{L}\right), \quad (41)$$

where H_A is the amplitude of the surface structure. We first consider the case in which the surface charge is distributed uniformly along the channel (Fig. 4(a)). We plot in Fig. 5 the flow rate for cases in which the mean salt concentration C_0 is 0.008, 0.032, and 0.128 mol/m³, as functions of the amplitude of the surface shape H_A in panel (a) and as functions of the geometrical parameter $\delta = \bar{H}/L$ in panel (b). The analytical results obtained from Eq. (40) are indicated by the solid lines, and the results of the numerical analysis obtained by using the LBM are indicated by the symbols. Whereas the analytical result is for the limit $\delta = \bar{H}/L \rightarrow 0$, the LBM simulations are performed for finite values of δ . The following parameters are used to characterize the electrolyte solution: $\rho_0 = 1 \times 10^3$ kg/m³, $\nu = 0.889 \times 10^{-6}$ m²/s, $D_a = D_c = 1 \times 10^{-8}$ m²/s, $-z_a = z_c = 1$, and $\varepsilon = 6.95 \times 10^{-10}$ C²/Jm. The temperature is 273 K, the strength of the external electric field is $\Delta\phi/L = 1 \times 10^4$ V/m, the constant surface charge density is $\sigma = -2 \times 10^{-5}$ C/m², and the mean channel width is $\bar{H} = 0.5 \mu\text{m}$. We note here that, with the above parameters, the Debye length (or the thickness of the electrical double layer) is comparable to the channel width, i.e., $\kappa \bar{H} = 4.86$ for $C_0 = 0.008$, $\kappa \bar{H} = 9.72$ for $C_0 = 0.032$, and $\kappa \bar{H} = 19.4$ for $C_0 = 0.128$ (see Eq. (23)).

Since the Debye length $1/\kappa$ shortens with the increase of the mean salt concentration and the electrical double layer becomes thin, less volume of the fluid feels the driving force due to the electric field for larger salt concentrations. The decrease of flow rate Q is therefore observed in Fig. 5(a), as the increase of salt concentration C_0 . Generally, the flow rate decreases with the increase of amplitude H_A ; that is, the electro-osmotic flow of the undulated surfaces is small compared with that of the straight channel ($H_A = 0$) having the width \bar{H} . This is consistent with the previous results, where the surface roughness is found to decrease the electro-osmotic flow rate [17, 20–22].

The analytical formula given in Eq. (40) is the flow rate in the limit of $\delta \rightarrow 0$. In other words, the frequency of the surface-shape variation is infinitesimal, because the surface shape is expressed in terms of the parameter δ as $h(x) = \bar{H} - H_A \cos(2\pi\delta x/\bar{H})$. Since the numerical data that are obtained for the finite values of δ properly converge to the analytical results with the decrease of δ , the appropriateness of analytical formula (40) is confirmed. The finite frequency effect decreases the flow rate, and the influence is larger for the larger values of amplitude H_A . We also plot in Fig. 5(b) the dependency on the parameter $\delta = \bar{H}/L$ at $H_A/\bar{H} = 0.4$. The deviation from the analytical value exhibits non-linear behavior, i.e., the flow rate quickly decreases for small values of δ and then gradually decays for large δ , which is consistent with the previous results, e.g., Fig. 3 of Ref. [21].

Before concluding this subsection, we briefly mention the computational system used in the the LBM. The lattice points are placed uniformly with lattice spacing $\Delta x/\bar{H} = 0.01$ (note that the lattice spacing divided by the characteristic length is of-

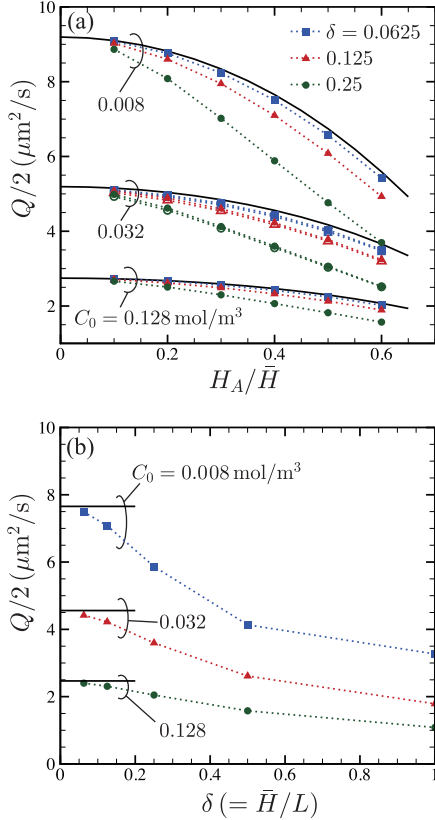


Figure 5: Electro-osmotic flow rate in the channel with undulated walls (a) as functions of H_A/\bar{H} and (b) as functions of δ at $H_A/\bar{H} = 0.4$. The surface charge density is constant ($\sigma = -2 \times 10^{-5} \text{ C/m}^2$). The solid lines indicate the analytical model in the limit of $\delta (= \bar{H}/L) \rightarrow 0$. The symbols indicate the results of the direct numerical simulation by using the LBM in the case of finite values of δ .

ten referred to as the Knudsen number in the LBM.) For example, in the case of $\delta = 0.0625$, 1600 lattice points are distributed along the x axis. We checked the sensitivity of the results on the size of the grid spacing by comparing the results with those under a coarser lattice system. The results with $\Delta x/\bar{H} = 0.02$ are shown for the case of $C_0 = 0.032 \text{ mol/m}^3$ in Fig. 5(a) by the open symbols. Since the results of $\Delta x/\bar{H} = 0.02$ are sufficiently close to those of $\Delta x/\bar{H} = 0.01$ (closed symbols), we safely use the latter grid spacing for all computations in the present paper. The time step used for electrolyte flow is $\Delta t_u = 0.0025 \text{ ns}$, and that for ion diffusion is $\Delta t_c = \Delta t_a = 0.25 \text{ ns}$. We note again that the difference comes from the large Schmidt number ($Sc \sim 90$), and $N_t = 100$ is chosen in the present work (See Fig. 2).

5.2. Inhomogeneously distributed surface charge

Next, we consider the case in which the surface charge is distributed along the channel, such that the net surface charge vanishes.

$$\int_0^L \sigma(x) dx = 0. \quad (42)$$

In this case, regions are charged positively and negatively, and the driving forces in the opposite directions are exerted if the external electric field is applied in the x direction. If the channel surfaces do not have the structure and the channel is straight, the

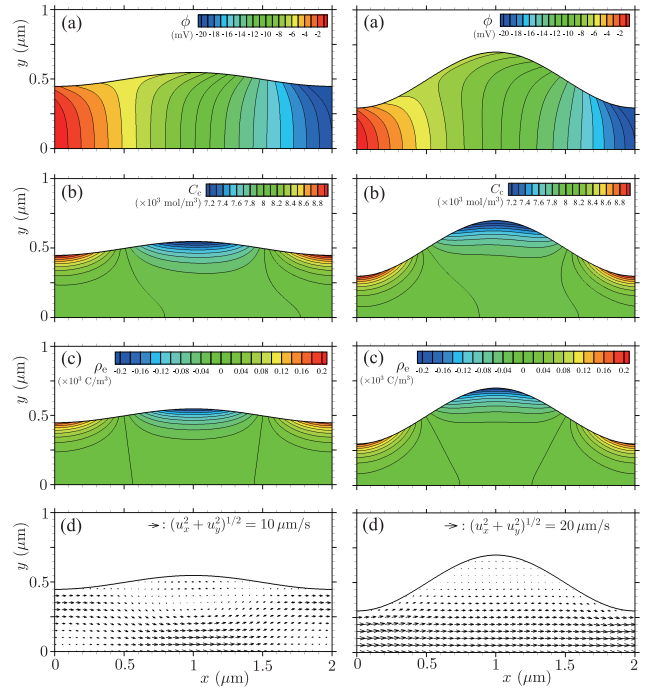


Figure 6: Two-dimensional plots of (a) electrical potential ϕ , (b) cation distribution C_c , (c) local charge density ρ_e , and (d) vector field \mathbf{u} , in the channel with inhomogeneous surface charge distribution. The average ion concentration is $C_0 = 0.008 \text{ mol/m}^3$, and the amplitude of the surface shape is $H_A/\bar{H} = 0.1$ (left panels), or $H_A/\bar{H} = 0.4$ (right panels).

driving forces in the opposite directions cancel and no net flow occurs in the x direction. However, if the surfaces are structured and the cross section varies along the channel, the symmetry of the forces can be broken and one-way flow in the x direction is expected. We note here that the idea of making one-way flows by means of the driving forces in the opposite directions has also been used in designing the Knudsen pump for a rarefied gas [53–56]. In the Knudsen pump, the thermal transpiration flows, which occur in opposite directions and are driven by the periodic temperature gradients, are used to extract a one-way flow by introducing the structured channel walls. The application of structured surfaces to induce one-way electro-osmotic flows was also proposed by Ajdari in Refs. [57, 58], under the assumption of infinitesimal thickness of the electrical double layer. Here we demonstrate the possibility of one-way flow in the case of the present setup, i.e., the thickness of the electrical double layer being comparable to the channel width.

We consider the case in which the surface charge $\sigma(x)$ is distributed along the channel as

$$\sigma(x) = \sigma_0 \cos\left(\frac{2\pi x}{L}\right), \quad (43)$$

where $\sigma_0 = -2 \times 10^{-5} \text{ C/m}^2$. As schematically shown in Fig. 4(b), the negatively charged region is narrower than the positively charged region, and the density of the driving force is larger in the negatively charged region. Hence, if the electric field is applied in the x direction, one-way flow is expected to take place

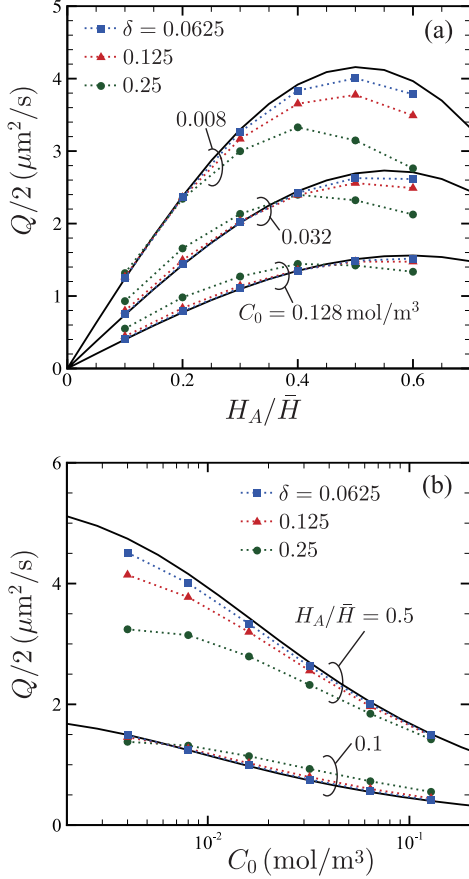


Figure 7: Electro-osmotic flow rate in the channel with undulated walls (a) as functions of the amplitude H_A/\bar{H} , and (b) as functions of the salt concentration C_0 . The surface charge is distributed inhomogeneously along the channel. See the caption of Fig. 5.

in the positive direction along the x axis, because the electrical double layer of the narrower region is positively charged. In Fig. 6, we show typical plots of electrical potential ϕ , cation distribution C_c , local charge density ρ_e , and flow velocity vector \mathbf{u} , obtained by using the LBM. The ion concentration is $C_0 = 0.008 \text{ mol/m}^3$, and the geometrical parameters are $\bar{H}/L = 0.25$, with $H_A/\bar{H} = 0.1$ (left panels), or with $H_A/\bar{H} = 0.4$ (right panels). The other parameters used are the same as those used in the previous subsection. Since the electric field is induced by the potential bias of $\Delta\phi = -20 \text{ mV}$ as shown in Figs. 6(a) the driving forces act in the positively and negatively charged regions shown in Figs. 6(c). Note that the asymmetric distribution of ion shown in Figs. 6(b) caused by the potential bias is not captured by the Poisson–Boltzmann formulation, because the Poisson–Boltzmann equation must be decoupled from the external electric field. The flow field in the case of small amplitude ($H_A/\bar{H} = 0.1$, the left panel of Fig. 6(d)) shows interference of the flows in the opposite directions and a vortex is observed around $x = 1 \mu\text{m}$. On the other hand, in the case of large amplitude ($H_A/\bar{H} = 0.4$, the right panel of Fig. 6(d)), the region where the driving force is exerted in the negative direction is mostly hidden inside the wider region, and strong one-way flow in the x direction occurs in the middle part of the channel.

To investigate the dependency of the electro-osmotic flow

rate on the geometrical parameter H_A , we consider the flow rate Q obtained from the LBM computations and that from the analytical formula given by Eq. (40) as functions of H_A , as shown in Fig. 7(a). In the case of the straight channel, i.e., $H_A = 0$, the flow rate is indeed zero, because the flows in the opposite directions cancel. The analytical results (Eq. (40)) indicated by the solid line show that the flow rate increases with the amplitude of the surface shape, and it peaks around $H_A/\bar{H} = 0.5\text{--}0.6$. The LBM results also show the same tendency, but the peaks shift slightly. It is also noted that for the cases of $C_0 = 0.032$ and 0.128 mol/m^3 , the effect of the finite value of δ raises the flow rate, i.e., that the fast variation of the surface shape and that of the surface charge density enlarge the electro-osmotic flow in these parameter ranges.

The analytical model (40) shows a strong non-linear dependency on important quantities such as dielectric constant ϵ , temperature T , and salt concentration C_0 , all through the inverse Debye length κ defined in Eq. (23). We plot in Fig. 7(b) the electro-osmotic flow rate as functions of C_0 to examine this dependency choosing C_0 as a controllable parameter. The flow rate slowly decreases with increasing C_0 thus with increasing κ (note the horizontal axis is in log scale). It is also observed that the effect of finite δ is significant for small values of C_0 with large amplitude H_A/\bar{H} .

The analysis of the problem considered in this section confirmed the occurrence of the one-way flow, even in the case of the zero net surface charge over the channel. In the next stage of our study, we will evaluate the possibility of the realization of one-way flow experimentally, and we will investigate applications of the present analysis methods to problems that include more complicated geometries, which we encounter in experimental setups such as porous media.

6. Conclusion

In the present study, we numerically investigated the electro-osmotic flows between two surfaces having a periodic structure by using the lattice Boltzmann method (LBM), and analytically by using the lubrication approximation theory for a moderate periodic structure. The numerical analysis is based on the coupled LBM framework developed in Ref. [24], where the Navier–Stokes equations for the fluid flow, the Nernst–Planck equation for the ion concentrations, and the Poisson equation for the electric field are simultaneously solved. In the latter analysis, a formula describing the electro-osmotic flow rate induced in the microchannel, which has a width comparable to the thickness of the electrical double layer, was derived for the first time for the case of structured surfaces and inhomogeneous surface charge distributions.

In the analysis of the electro-osmotic flow through channels with the undulated surfaces charged at a constant surface charge density, the flow rate was found to be suppressed by the large surface structure, even for the infinitely slow variation of the surface shape. The LBM results for the finite frequency of the surface-shape variation showed that the fast variation of the surface shape further decreases the flow rate. The analysis of the inhomogeneously distributed surface charge confirmed

the occurrence of the one-way flow, even under the constraint of the zero net surface charge over the channel. These results could pave the way for the design of novel devices utilizing the electrokinetic flows in microchannels.

Acknowledgments

The authors thank S. Iwai for computer assistance. The present work was partially supported by the MEXT program “Elements Strategy Initiative to Form Core Research Center” (since 2012). (MEXT: Ministry of Education, Culture, Sports, Science, and Technology, Japan.)

References

- [1] J. N. Israelachvili, *Intermolecular and surface forces* 3rd Edition, Academic press, 2011.
- [2] G. Karniadakis, A. Beskok, N. Aluru, *Microflows and Nanoflows*, Springer, 2005.
- [3] J. P. Urbanski, T. Thorsen, J. A. Levitan, M. Z. Bazant, Fast ac electro-osmotic micropumps with nonplanar electrodes, *Appl. Phys. Lett.* 89 (2006) 143508.
- [4] Q. Yuan, J. Wu, Thermally biased ac electrokinetic pumping effect for lab-on-a-chip based delivery of biofluids, *Biomed. Microdevices* 15 (2013) 125–133.
- [5] A. Siria, P. Poncharal, A.-L. Biance, R. Fulcrand, X. Blase, S. T. Purcell, L. Bocquet, Giant osmotic energy conversion measured in a single transmembrane boron nitride nanotube, *Nature* 494 (2013) 455–458.
- [6] Z. Chai, Z. Guo, B. C. Shi, Study of electro-osmotic flows in microchannels packed with variable porosity media via lattice Boltzmann method, *J. Appl. Phys.* 101 (10) (2007) 104913.
- [7] R. B. Schoch, J. Han, P. Renaud, Transport phenomena in nanofluidics, *Rev. Mod. Phys.* 80 (2008) 839–883.
- [8] L. Bocquet, E. Charlaix, Nanofluidics, from bulk to interfaces, *Chem. Soc. Rev.* 39 (2010) 1073–1095.
- [9] C. Zhao, C. Yang, Advances in electrokinetics and their applications in micro/nano fluidics, *Microfluid. Nanofluid.* 13 (2012) 179–203.
- [10] R. Dey, T. Ghonge, S. Chakraborty, Steric-effect-induced alteration of thermal transport phenomenon for mixed electroosmotic and pressure driven flows through narrow confinements, *Int. J. Heat Mass Transf.* 56 (2013) 251–262.
- [11] J. Zudrop, S. Roller, P. Asinari, Lattice Boltzmann scheme for electrolytes by an extended Maxwell–Stefan approach, *Phys. Rev. E* 89 (2014) 053310.
- [12] H. Yoshida, H. Mizuno, T. Kinjo, H. Washizu, J.-L. Barrat, Molecular dynamics simulation of electrokinetic flow of an aqueous electrolyte solution in nanochannels, *J. Chem. Phys.* 140 (2014) 214701.
- [13] H. Yoshida, H. Mizuno, T. Kinjo, H. Washizu, J.-L. Barrat, Generic transport coefficients of a confined electrolyte solution, *Phys. Rev. E* 90 (2014) 052113.
- [14] A. Mehboudi, M. Noruzitabar, M. Mehboudi, Simulation of mixed electroosmotic/pressure-driven flows by utilizing dissipative particle dynamics, *Microfluid. Nanofluid.* 17 (2014) 199–215.
- [15] D. V. Patil, K. N. Premnath, D. Desai, S. Banerjee, Electrodeposition modeling using coupled phase-field and lattice Boltzmann approach, *Int. J. of Mod. Phys. C* 25 (2014) 1340018.
- [16] F. Tessier, G. W. Slater, Modulation of electroosmotic flow strength with end-grafted polymer chains, *Macromolecules* 39 (2006) 1250–1260.
- [17] M. Wang, J. Wang, S. Chen, Roughness and cavitations effects on electro-osmotic flows in rough microchannels using the lattice Poisson-Boltzmann methods, *J. Comput. Phys.* 226 (2007) 836–851.
- [18] M. Wang, Q. Kang, Electrokinetic transport in microchannels with random roughness, *Anal. Chem.* 81 (2009) 2953–2961.
- [19] Z. Xia, R. Mei, M. Sheplak, Z. H. Fan, Electroosmotically driven creeping flows in a wavy microchannel, *Microfluid. Nanofluid.* 6 (2009) 37–52.
- [20] S. Bhattacharyya, A. K. Nayak, Combined effect of surface roughness and heterogeneity of wall potential on electroosmosis in microfluidic/nanofluidic channels, *J. Fluid. Eng.* 132 (2010) 041103.
- [21] R. J. Messinger, T. M. Squires, Suppression of electro-osmotic flow by surface roughness, *Phys. Rev. Lett.* 105 (2010) 144503.
- [22] J. Liu, M. Wang, S. Chen, M. O. Robbins, Molecular simulations of electroosmotic flows in rough nanochannels, *J. Comput. Phys.* 229 (2010) 7834–7847.
- [23] S. Bhattacharyya, S. Bera, Combined electroosmosis-pressure driven flow and mixing in a microchannel with surface heterogeneity, *Appl. Math. Model.* in press. doi:doi:10.1016/j.apm.2014.12.050.
- [24] H. Yoshida, T. Kinjo, H. Washizu, Coupled lattice Boltzmann method for simulating electrokinetic flows: a localized scheme for the Nernst–Planck model, *Commun. Nonlinear Sci. Numer. Simulat.* 19 (2014) 3570–3590.
- [25] S. Ghosal, Lubrication theory for electro-osmotic flow in a microfluidic channel of slowly varying cross-section and wall charge, *J. Fluid Mech.* 459 (2002) 103–128.
- [26] C.-O. Ng, Q. Zhou, Electro-osmotic flow through a thin channel with gradually varying wall potential and hydrodynamic slippage, *Fluid Dyn. Res.* 44 (2012) 055507.
- [27] C.-O. Ng, C. Qi, Electroosmotic flow of a power-law fluid in a non-uniform microchannel, *J. Non-Newtonian Fluid Mech.* 208 (2014) 118–125.
- [28] J. Newman, *Electrochemical Systems*, 2nd Edition, Prentice-Hall, Englewood Cliffs, NJ, 1991.
- [29] G. R. McNamara, G. Zanetti, Use of the Boltzmann equation to simulate lattice-gas automata, *Phys. Rev. Lett.* 61 (1988) 2332.
- [30] Y. H. Qian, D. d’Humières, P. Lallemand, Lattice BGK models for Navier–Stokes equation, *Europhys. Lett.* 17 (1992) 479.
- [31] S. Chen, G. D. Doolen, Lattice Boltzmann method for fluid flows, *Annu. Rev. Fluid Mech.* 30 (1998) 329–364.
- [32] S. Succi, *The lattice Boltzmann equation for fluid dynamics and beyond*, Oxford Univ. Press, New York, 2001.
- [33] P. Lallemand, L.-S. Luo, Theory of the lattice Boltzmann method: Dispersion, dissipation, isotropy, Galilean invariance, and stability, *Phys. Rev. E* 61 (2000) 6546–6562.
- [34] D. d’Humières, I. Ginzburg, M. Krafczyk, P. Lallemand, L.-S. Luo, Multiple-relaxation-time lattice Boltzmann models in three dimensions, *Philos. Trans. R. Soc. Lond. A* 360 (2002) 437–451.
- [35] S. Ansumali, I. V. Karlin, H. C. Öttinger, Minimal entropic kinetic models for hydrodynamics, *Europhys. Lett.* 63 (2003) 798.
- [36] M. Geier, A. Greiner, J. G. Korvink, Cascaded digital lattice Boltzmann automata for high Reynolds number flow, *Phys. Rev. E* 73 (2006) 066705.
- [37] I. Ginzburg, Truncation errors, exact and heuristic stability analysis of two-relaxation-times lattice Boltzmann schemes for anisotropic advection-diffusion equation, *Commun. Comput. Phys.* 11 (2012) 1439.
- [38] Z. Guo, C. Zheng, B. C. Shi, Lattice Boltzmann equation with multiple effective relaxation times for gaseous microscale flow, *Phys. Rev. E* 77 (2008) 036707.
- [39] H. Yoshida, M. Nagaoka, Multiple-relaxation-time lattice Boltzmann model for the convection and anisotropic diffusion equation, *J. Comput. Phys.* 229 (2010) 7774–7795.
- [40] T. Gebäck, A. Heintz, A lattice Boltzmann method for the advection-diffusion equation with Neumann boundary conditions, *Commun. Comput. Phys.* 15 (2013) 487–505.
- [41] L. Li, R. Mei, J. F. Klausner, Boundary conditions for thermal lattice Boltzmann equation method, *J. Comput. Phys.* 237 (2013) 366–395.
- [42] X. He, L.-S. Luo, Lattice Boltzmann model for the incompressible Navier–Stokes equation, *J. Stat. Phys.* 88 (1997) 927–944.
- [43] Y. H. Qian, S. A. Orszag, Lattice BGK models for the Navier–Stokes equation: Nonlinear deviation in compressible regimes, *Europhys. Lett.* 21 (1993) 255–259.
- [44] M. Wang, Q. Kang, Modeling electrokinetic flows in microchannels using coupled lattice Boltzmann methods, *J. Comput. Phys.* 229 (2010) 728–744.
- [45] F. Capuani, I. Pagonabarraga, D. Frenkel, Discrete solution of the electrokinetic equations, *J. Chem. Phys.* 121 (2004) 973–986.
- [46] I. Pagonabarraga, F. Capuani, D. Frenkel, Mesoscopic lattice modeling of electrokinetic phenomena, *Comput. Phys. Commun.* 169 (2005) 192–196.
- [47] Z. Guo, T. S. Zhao, Y. Shi, A lattice Boltzmann algorithm for electroosmotic flows in microfluidic devices, *J. Chem. Phys.* 122 (2005) 144907.
- [48] Z. Chai, B. Shi, Simulation of electro-osmotic flow in microchannel with lattice Boltzmann method, *Phys. Lett. A* 364 (2007) 183–188.

- [49] J. Wang, M. Wang, Z. Li, Lattice evolution solution for the nonlinear Poisson-Boltzmann equation in confined domains, *Commun. Nonlinear Sci. Numer. Simulat.* 13 (2008) 575–583.
- [50] J. Zhang, Lattice Boltzmann method for microfluidics: models and applications, *Microfluid. Nanofluid.* 10 (2011) 1–28.
- [51] Z. Chai, B. C. Shi, A novel lattice Boltzmann model for the Poisson equation, *Appl. Math. Model.* 32 (2008) 2050–2058.
- [52] D. V. Patil, K. N. Premnath, S. Banerjee, Multigrid lattice Boltzmann method for accelerated solution of elliptic equations, *J. Comput. Phys.* 265 (2014) 172–194.
- [53] Y. Sone, Y. Waniguchi, K. Aoki, One-way flow of a rarefied gas induced in a channel with a periodic temperature distribution, *Phys. Fluids* 8 (1996) 2227–2235.
- [54] K. Aoki, P. Degond, S. Takata, H. Yoshida, Diffusion models for Knudsen compressors, *Phys. Fluids* 19 (2007) 117103,p1–p21.
- [55] K. Aoki, P. Degond, L. Mieussens, S. Takata, H. Yoshida, A diffusion model for rarefied flows in curved channels, *Multiscale Model. Simul.* 6 (2008) 1281–1316.
- [56] K. Aoki, S. Takata, E. Tatsumi, H. Yoshida, Rarefied gas flows through a curved channel: Application of a diffusion-type equation, *Phys. Fluids* 22 (2010) 112001.
- [57] A. Ajdari, Electro-osmosis on inhomogeneously charged surfaces, *Phys. Rev. Lett.* 75 (1995) 755–758.
- [58] A. Ajdari, Generation of transverse fluid currents and forces by an electric field: Electro-osmosis on charge-modulated and undulated surfaces, *Phys. Rev. E* 53 (1996) 4996.